Improvements to Image Processing in the DES-GW Pipeline

Noemi Glaeser*[1,2] and Kenneth Herner[2]

[1]*Department of Computer Science, University of South Carolina, Columbia, SC*
[2]*Fermi National Accelerator Laboratory, Batavia, IL*

Submitted: 10 August 2018

Abstract

Gravitational wave (GW) events caused by binary neutron star (BNS) mergers are known to have observable electromagnetic counterparts. The DES-GW group, consisting of members of the Dark Energy Survey (DES), Laser Interferometer Gravitational Wave Observatory (LIGO), and the astronomical community, attempts to locate and observe these counterparts upon LIGO detection of a BNS event. DES employs a series of computer programs, known as the DES-GW pipeline, to capture and process Dark Energy Camera (DECam) images of the counterpart's probability region with the goal of identifying the exact location and characteristics of the GW event counterpart. This paper describes improvements made to the image processing portion of the DES-GW pipeline before LIGO Observing Run 3 (O3) in 2019.
Keywords: Gravitational waves (GW), bright standard sirens, DECam, kilonova, binary neutron star (BNS), Hubble constant

1 Introduction

Precision cosmology generally employs a cosmic distance ladder, which is imprecise and introduces systemic uncertainties. With the discovery of Type Ia supernovae, a new measure of distance was discovered. Recently, another measure of distance has emerged through gravitational wave detectors like the Laser Interferometer Gravitational-Wave Observatory (LIGO). By observing gravitational waves (GW) emitted by the distant mergers of massive objects, LIGO can measure the distance directly to these events. Observing the same object in the optical range (*i.e.*, the kilonova) allows us to gather additional information about the event, including redshift, which leads to improved constraints on cosmological parameters such as the Hubble constant and the cosmological constant.

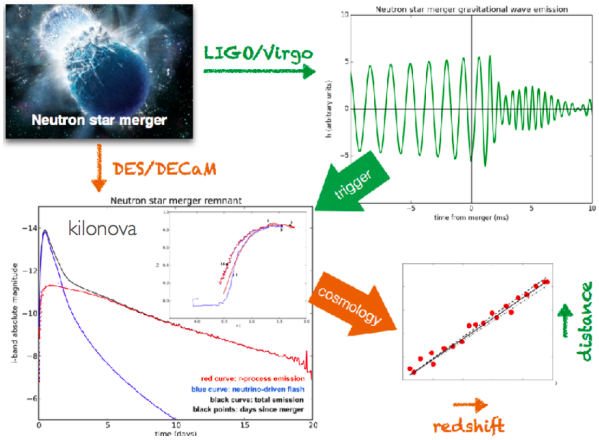

Figure 1: A BNS event leads to both GW and EM detection. Through these observations, we determine redshift and distance which helps to characterize the cosmology, for instance by placing further bounds on the value of the Hubble constant. Image from Soares-Santos [1].

1.1 Gravitational waves and Cosmological Parameters

LIGO detects major events such as binary black hole (BBH), binary neutron star (BNS), and neutron star-black hole (NS-BH) mergers by observing the gravitational waves emitted. So far, only BNS mergers are known to produce electromagnetic radiation in the optical range, known as a kilonova. Just as Type Ia supernovae have a known luminosity (hence the term "standard candle") and thus led to measurement of the Hubble constant, kilonovae have a known distance measured through analysis of their gravitational waveforms and are also visible in the EM spectrum (hence the name "bright standard sirens").

To measure the Hubble constant H_0, a distance-redshift plot is made. In the case of Type Ia supernovae, the distance is found by comparing the measured luminosity to the known luminosity at the source. Bright standard sirens, on the other hand, have an independent distance measurement which comes directly from the observed GW. Determining the Hubble constant in this second, independent way allows us to place better constraints on its value. Additional observations from the electromagnetic counterparts also help us improve constraints on other cosmological parameters such as the matter density of the universe, Ω_M, and the cosmological constant, Ω_Λ. This process is described in Figure 1.

1.2 The Dark Energy Survey

The Dark Energy Survey is a collaboration which uses various observables to gain a better understanding of

*Corresponding author: nglaeser@email.sc.edu

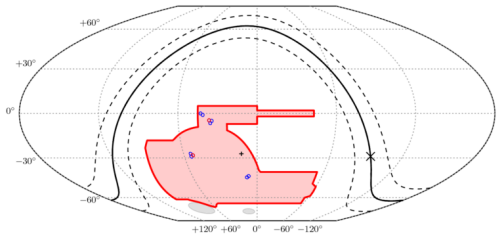

Figure 2: The 5000 square degree DES DR1 footprint. The blue and red circles indicate the shallow and deep supernova fields, respectively. The solid line represents the Milky Way with a 20 degree margin (dashed lines). The galactic center (x), South Pole (+), and Small and Large Magellanic Clouds (gray) are shown as well. Image from Dark Energy Survey [2].

dark energy through cosmology. The images taken over the course of the survey are analyzed for phenomena such as weak lensing and galaxy clusters.

Recently, GW counterparts have become of interest as another observable to glean insight on the nature of dark energy, which is described by the Hubble constant and the aforementioned cosmological parameters. Upon detection of a GW event, LIGO alerts the public with information about the event, including a probability region of event's location, the type of event, and its distance. DES then uses this information to search for the counterpart by imaging the sky in the probability region as part of a special target of opportunity (TOO) observing time (separate from the pre-planned survey nights).

1.2.1 DECam

Our instrument is the Dark Energy Camera (DECam), a 570 megapixel 2.2-degree field-of-view camera mounted on the 4-meter Blanco telescope at the Cerro Tololo Inter-American Observatory (CTIAO) in Chile [3, 4]. DECam possesses 62 charge-coupled devices (CCDs) used in data analysis which can observe the sky in six filters (u, g, r, i, z, and Y). Over the course of the 525-night survey, it will cover the 500-square-degree DES footprint (see Figure 2) ten times in each of the g, r, i, and z bands [2–4].

1.2.2 Image processing

We process images from the DECam on the Open Science Grid (OSG) using our image processing pipeline (a subsection of the full DES-GW pipeline). On the night of a LIGO trigger, each exposure is passed to the image processing pipeline, consisting of a single-epoch (SE) and `DiffImg` processing stage.

The SE pipeline processes raw exposures from DECam into science-ready images. These are then passed to the `DiffImg` pipeline, where we compare the image (known as the "search image" to template images of the same area of the sky taken either before or after the search image (on normal, *i.e.* non-trigger, nights). We subtract the template images from the search image to obtain a difference image, from which we extract candidate counterpart objects [5]. The image processing pipeline is further described in Section 2.

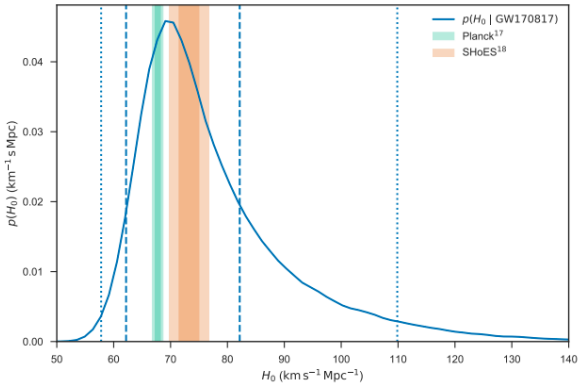

Figure 3: Plot of the third independent H_0 measurement from GW170817 overlaid on the two previous values. With more GW events, the uncertainty of the GW H_0 value will be reduced with the goal of discriminating between the disparate measurements by SHoES and Planck. Figure from Abbott et al. [6].

1.2.3 GW170817

In August of 2017, the DES-GW group observed the first optical counterpart of a GW event, GW170817[3, 7]. This served as a single point on the redshift-distance plot (see Figure 1) and gave a third independent measurement of the Hubble constant (Figure 3).

In this run, each exposure was processed within 5-8 hours (from acquisition to candidate list). As the number of LIGO events is expected to increase significantly in O3, we sought to reduce the image processing time to less than one hour.

2 Methods

In this paper we describe improvements made to the performance of the image processing pipeline. The pipeline has two stages: single epoch (SE) processing and difference imaging with `DiffImg`.

2.1 SE Processing

SE processing consists of an image correction stage and an image calibration stage. This used to be done sequentially for each CCD and took about 1 hour per image (though images can be processed in parallel). By modifying the calibration stage to run in parallel on each CCD we allow each processed CCD image to immediately proceed to the difference imaging stage. Thus difference imaging on single CCDs can begin before the entire exposure has finished SE processing. In the new SE processing, one CCD averaged 0.15 hours.

Previously, both astrometric and photometric image calibration utilized the 2MASS star catalog. This catalog has a high uncertainty for faint stars. In addition, its epoch (year ∼2000) is far enough removed

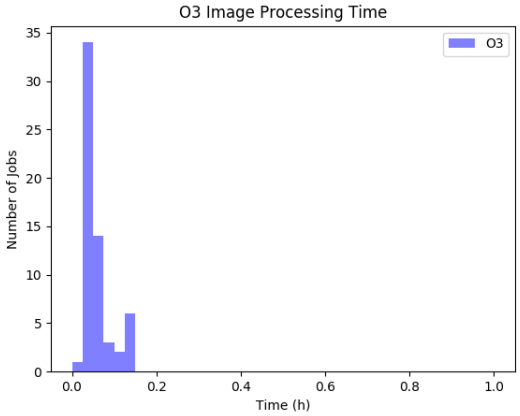

Figure 4: O3 image processing pipeline times for one exposure in a grid job (60 CCDs processed in parallel; $\mu = 0.05$, median= 0.04, $\sigma = 0.03$). Decreased from 5-8 hours per exposure.

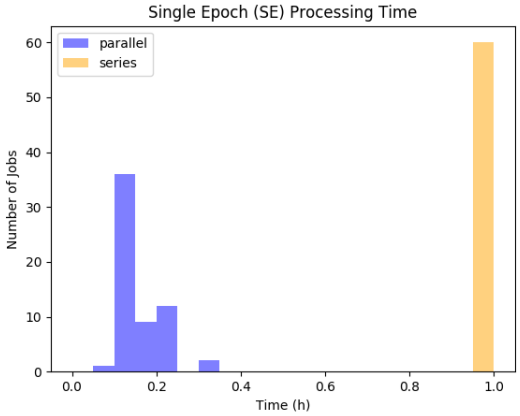

Figure 5: Comparison of SE processing runtime (subsection of the image processing pipeline) in a grid computing job with 60 CCDs in series (yellow; 0.9625) and in parallel (purple; $\mu = 0.15$, median= 0.13, $\sigma = 0.05$). These times were obtained after initial parallelization; further modifications in the full pipeline further reduced processing time, leading to even shorter run of full image processing (Figure 4).

from the DES epoch (year ∼2015) to contribute to astrometric uncertainties[8]. In addition, its density is insufficient for single-CCD calibration. Thus we adapted the calibration steps to use the newer GAIA-DR2 catalog (released April 25, 2018) for both template and search images[9, 10].

2.2 Difference imaging

The bulk of the `DiffImg` pipeline consists of 28 steps. These include conducting another astrometric calibration with the SCAMP package (steps 7-8), injecting fake objects to later use in performance evaluation (step 11), using the HOTPANTS package to subtract template images from the search image (step 18), generating a list of candidate objects from the difference image with SExtractor (step 20), running these objects through a machine learning algorithm to determine their likelihood (between 0 and 1) of being the counterpart (step 21), and finally writing all this information to the DES-GW database (steps 22-28).

The `DiffImg` pipeline had already been implemented to run in parallel per CCD in O1 and O2[8]. Since we adapted SE processing to run on a per-CCD basis, we were able to eliminate intermediate verfication steps taken between the SE processing and difference imaging steps by modifying the pipeline to flow directly from the former into the latter.

2.3 Pipeline Integration

After all modifications were made, the full image-processing pipeline was integrated into one workflow from raw image to candidate list.

3 Results

3.1 Timing

The modified image processing portion of the DES-GW pipeline, from raw image to candidate list, takes ∼0.2 hours in a grid computing job for a single exposure (60 CCDs) (Figure 4). This is a significant decrease from the O2 pipeline, which took between 5 and 8 hours for this portion (factor of 25-40 speedup). The speedup is largely due to the parallelization of the SE portion. A comparison of series and parallel SE processing times is shown in Figure 5. On average, parallelization resulted in approximately a factor of 6 speedup of SE processing.

3.2 Accuracy

The modified pipeline still identifies the GW170817 counterpart. It performed admirably (hopefully) in our mock observing run. A comparison of the candidates identified by the O2 pipeline in exposure 668439 (the area containing the GW170817 counterpart) and the new O3 pipeline is shown in Figure 6. Although only 75.8% of O2 candidates were also identified by O3 (*i.e.* 37 O2 candidates were not identified by O3) and O3 identified 27 candidates not found by O2, only 10 of these unmatched objects had an ML score above 0.5

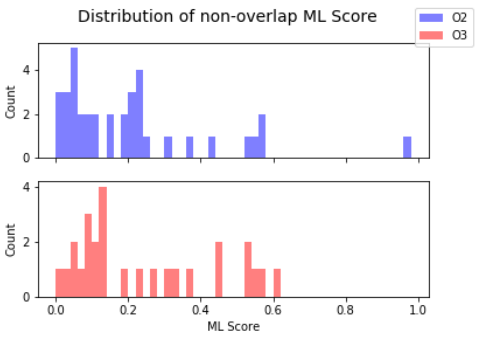

Figure 8: ML scores of the unmatched candidate objects in the O2 and O3 pipelines.

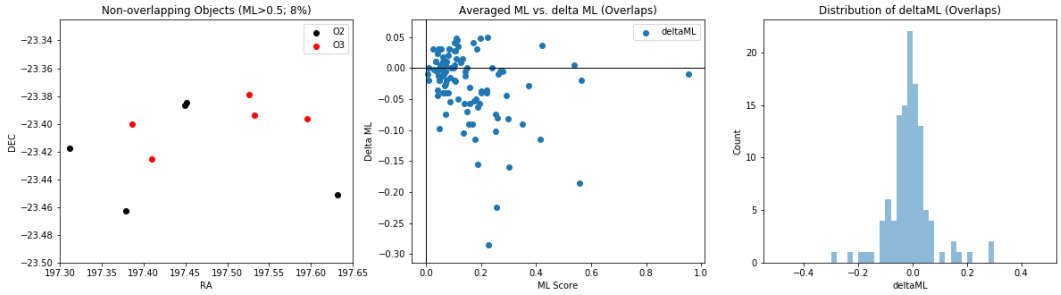

Figure 6: Summary of comparison between 2MASS-calibrated processing (O2 pipeline) and GAIA-calibrated processing (O3 pipeline). Left: location of candidates with ML> 0.5 not identified by both pipelines; Center: Difference in ML scores assigned to candidates by each pipeline as a function of average score; Right: Distribution of ML score differences.

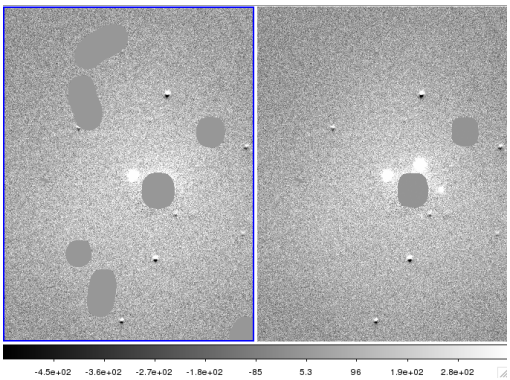

Figure 7: Comparison of difference images for new O3 SE-processed (left) and O2 SE-processed candidate image. The candidate is still identified in both (bright spot in the center) but the left image identifies fewer false candidates.

and only 1 above 0.7. This indicates that a majority of the unmatched objects were not viable candidates and unlikely to be the true counterpart (see Figure 8).

The unmatched false counterpart with the highest ML score (ML=0.96) was identified by the O2 pipeline and not by the O3 pipeline. It was present in both the i and z of the O2-processed difference image for exposure 668439, but absent in both the O3 i and z difference images. The object was not present in an O2 difference image of the same area of the sky and same night with a slightly different camera pointing (exposure 668443), leading us to believe it was an anomaly in the exposure. In O2, the object was ultimately eliminated as the counterpart with later cuts because it did not appear to have a host galaxy and did not fade over a time scale characteristic of a kilonova (see Soares-Santos et al. [3] for details). As such, we conclude that its absence in the O3 candidate list is not indicative of an overall failure by the modified pipeline and was most likely an anomaly in the combination of O2 processing and exposure.

The changes in the O3 processing pipeline also led to minimal differences in machine learning (ML) scores as shown in the center and right panels of the image. In general, the O3 pipeline assigned more conservative ML scores, as indicated by the left-skewed normal distribution.

Since the O3 pipeline still identified the counterpart, we conclude that the new SE processing acted favorably by identifying fewer false candidates with high ML scores. The resulting difference images are shown in Figure 7.

4 Conclusions

The entire DES-GW image processing pipeline, from raw image to candidate list, now runs in 0.2 hours for a single exposure. This is a factor of 25-40 speedup and meets our goal of running within 1 hour. It will be used in LIGO O3 in early 2019 will be instrumental in handling the expected tenfold increase in GW events.

Acknowledgements

This document was prepared by the authors using the resources of the Fermi National Accelerator Laboratory (Fermilab), a U.S. Department of Energy, Office of Science, HEP User Facility. Fermilab is managed by Fermi Research Alliance, LLC (FRA), acting under Contract No. DE-AC02-07CH11359.

Additionally, this work has made use of data from the European Space Agency (ESA) mission *Gaia* (https://www.cosmos.esa.int/gaia), processed by the *Gaia* Data Processing and Analysis Consortium (DPAC, https://www.cosmos.esa.int/web/gaia/dpac/consortium). Funding for the DPAC has been provided by national institutions, in particular the institutions participating in the *Gaia* Multilateral Agreement.

Noemi Glaeser was funded by Fermilab's Summer Internship in Science and Technology (SIST) program and the Scientific Computing Division. Thanks also to Kenneth Herner, James Annis, and Marcelle Soares-Santos for their guidance, and to the 2018 DES-GW interns for sharing their knowledge (in particular Nora Sherman and Alyssa Garcia).

References

[1] M. Soares-Santos, Observation of a gravitational wave emitting neutron star merger with the dark

energy camera (2017), http://vms.fnal.gov/asset/detail?recid=1951208.

[2] Dark Energy Survey, The DES project: Overview (2018), https://www.darkenergysurvey.org/the-des-project/overview/.

[3] M. Soares-Santos, D. E. Holz, J. Annis, R. Chornock, K. Herner, E. Berger, D. Brout, H.-Y. Chen, R. Kessler, M. Sako, et al., The electromagnetic counterpart of the binary neutron star merger ligo/virgo gw170817. i. discovery of the optical counterpart using the dark energy camera, *The Astrophysical Journal Letters* **848**, L16 (2017).

[4] B. Flaugher, H. T. Diehl, K. Honscheid, T. M. C. Abbott, O. Alvarez, R. Angstadt, J. T. Annis, M. Antonik, O. Ballester, L. Beaufore, et al., The dark energy camera, *AJ* **150**, 150 (2015), arXiv:1504.02900.

[5] R. Kessler, J. Marriner, M. Childress, R. Covarrubias, C. B. D'Andrea, D. A. Finley, J. Fischer, R. J. Foley, D. Goldstein, R. R. Gupta, et al., The difference imaging pipeline for the transient search in the dark energy survey, *AJ* **150**, 172 (2015).

[6] B. P. Abbott et al. (LIGO Scientific, VINROUGE, Las Cumbres Observatory, DES, DLT40, Virgo, 1M2H, Dark Energy Camera GW-E, MASTER), A gravitational-wave standard siren measurement of the Hubble constant, *Nature* **551**, 85 (2017), arXiv:1710.05835.

[7] B. P. Abbott, R. Abbott, T. D. Abbott, F. Acernese, K. Ackley, C. Adams, T. Adams, P. Addesso, R. X. Adhikari, V. B. Adya, et al., Multi-messenger observations of a binary neutron star merger, *The Astrophysical Journal Letters* **848**, L12 (2017).

[8] K. Herner, M. Soares-Santos, J. Annis, D. Brout, R. Kessler, M. Sako, R. Butler, Z. Doctor, A. Palmese, H. Chen, et al., Optical follow-up of gravitational wave triggers with decam: the details paper (2018).

[9] Gaia Collaboration, Prusti, T., de Bruijne, J. H. J., Brown, A. G. A., Vallenari, A., Babusiaux, C., Bailer-Jones, C. A. L., Bastian, U., Biermann, M., Evans, D. W., et al., The gaia mission, *A&A* **595**, A1 (2016).

[10] Gaia Collaboration, A. G. A. Brown, A. Vallenari, T. Prusti, J. H. J. de Bruijne, C. Babusiaux, and C. A. L. Bailer-Jones, Gaia Data Release 2. Summary of the contents and survey properties, *ArXiv e-prints* (2018), arXiv:1804.09365.